ELECTRONIC SUPPLEMENTARY INFORMATION

Nanoscale solvent organization in metal-organic framework ZIF-8 probed by EPR of flexible β-phosphorylated nitroxides

Artem S. Poryvaev,[a] Aleksandr A. Efremov,[a,b] Dmitry V. Alimov, [a,b] Kristina A. Smirnova,[a,b] Daniil M. Polyukhov,[a] Renad Z. Sagdeev,[a] Samuel Jacoutot,[c] Sylvain R. A. Marque,[c,*] Matvey V. Fedin [a,b,*]

[a]International Tomography Center SB RAS, Novosibirsk, 630090, Russia; mfedin@tomo.nsc.ru
[b]Novosibirsk State University, Novosibirsk, 630090, Russia
[c]Aix Marseille University, CNRS, UMR Avenue Escadrille Normandie-Niemen 7273 Marseille, 13397 cedex 20, France; sylvain.marque@univ-amu.fr

Table of contents:

I. PXRD data

The studied sample S1@ZIF-8 was characterized by powder X-ray diffraction (PXRD). The PXRD pattern (Fig. S1, black) showed typical 2θ peak positions for ZIF-8. Peak positions correspond well to the simulated PXRD data for ZIF-8 obtained using Mercury 3.3 (Fig. S1, blue).

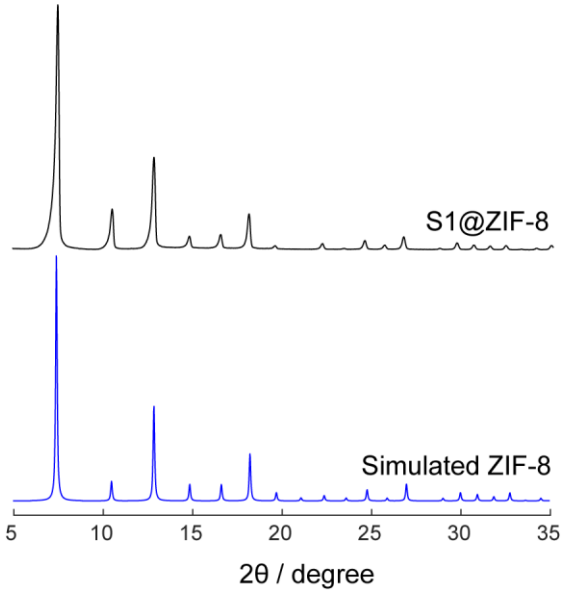

Figure S1. PXRD data for S1@ZIF-8 (black) and ZIF-8 simulated by Mercury 3.3 (blue).

Impregnation of S1@ZIF-8 with various solvents did not lead to any modification or destruction of the MOF structure. Figure S2 evidences this using MeOH as an example.

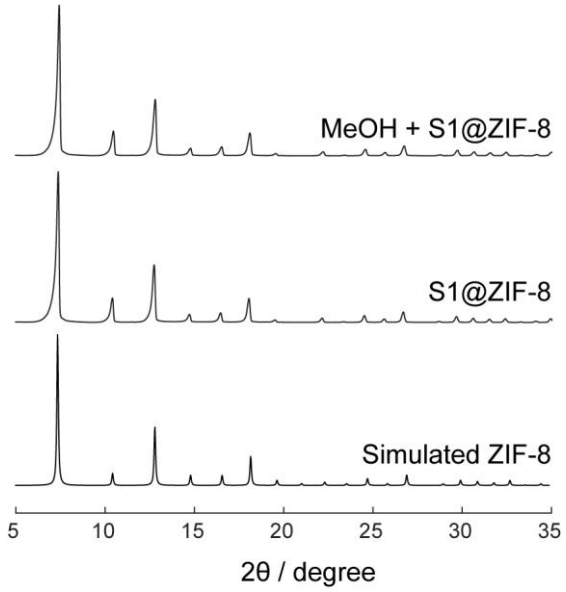

Figure S2. PXRD data for S1@ZIF-8, S1@ZIF-8 after methanol treatment and pattern simulated by Mercury 3.3.

II. DFT studies

II.1. Dependence of A_P on θ

We investigated the dependence of isotropic HFI constants A_N and A_P on the geometry of the radical.

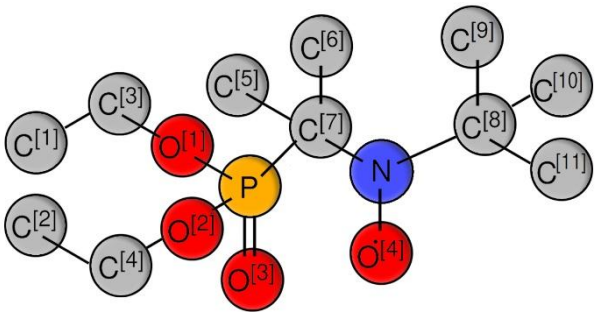

Figure S3. Atomic scheme of studied β-phosphorylated nitroxide radical. Hydrogens are not shown.

We found the equilibrium geometry of the radical using B3LYP/TZVP with RIJCOSX approximation, def2/J auxiliary basis set. To establish qualitative dependences, it can be assumed that SOMO of nitrogen is perpendicular to the N-O bond, therefore the angle θ can be estimated according to equation (S1).

$$\theta \approx \widehat{\overrightarrow{O^{[4]}N}, \overrightarrow{C^{[7]}P}} + \frac{\pi}{2} = \theta_{appox} \qquad \text{(S1)}$$

Therefore, we first scanned radical geometry changing $\theta \approx \theta_{approx}$. For each optimized geometry, A_P hyperfine interaction constants were calculated using TPSS / def2-TZVPD. The experimental points (taken from Table 1 and from Tables S3-S4) qualitatively coincide with the DFT calculation. (Fig. S4a).

II.2. Influence of various geometric parameters on A_P and its dependence on θ

We selected geometric parameters (bond lengths, angles, dihedrals) which have the greatest impact on the values A_N and A_P (Table S2) and monitored how additional geometric constraints affect the dependence of A_P on θ. In each case we varied the values of the selected geometric parameters around their equilibriums in reasonable ranges and calculated the dependence of A_P on angle θ (more precisely, on $\cos^2\theta$).

Figure S4 shows the dependence of A_P on $\cos^2\theta$ for equilibrium parameters, which is in reasonably good agreement with experimental data.

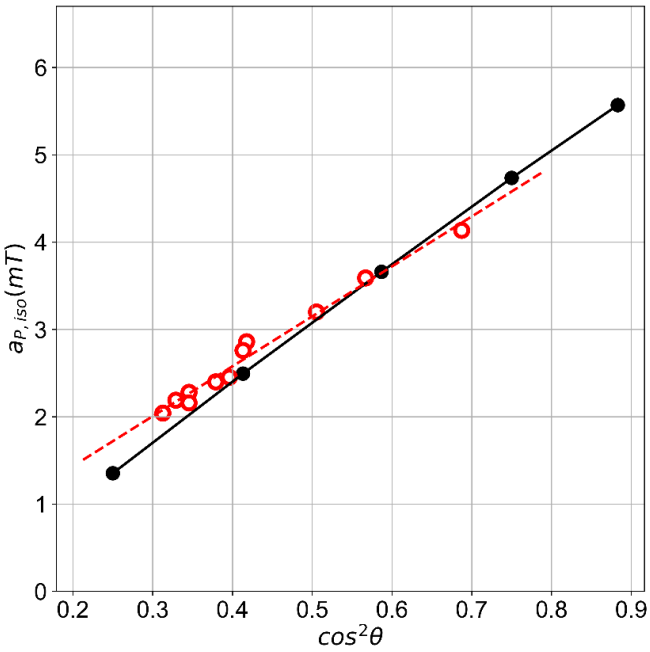

Figure S4. Dependence of A_P on $\cos^2\theta$ for equilibrium parameters. Experimental points are shown by red circles. Dashed line represents a linear trend of experimental points.

Dihedral angles were varied in 15-degree increment from -30 to +30 relative to equilibrium value. Bond lengths were scanned over a range of 5% of the equilibrium length in 2.5% increment (variations in normal conditions depending on solvent polarity are expected to be smaller). Angles were scanned over a range of 15% around the equilibrium value in 7.5% increment. Table S1 and Fig.S3 explain which angles, bond lengths and dihedrals were varied.

Table S1. Geometric parameters varied around their equilibrium values. Corresponding color codes used in Fig.S5 are indicated.

Bonds			**Angles**			**Dihedrals**	
atoms	**Color (Fig. S5a)**		**atoms**	**Color (Fig. S5b)**		**atoms**	**Color (Fig. S5c)**
NO^4	Red		O^4NC^8	Red		NC^7PO^3	Red
NC^7	Green		C^8NC^7P	Green		C^8NC^7P	Green
PO^3	Blue		$O^4NC^7C^{5/6}$	Blue		$O^4NC^7C^{5/6}$	Blue
PC^7	Magenta		C^7PO^3	Magenta		O^4NC^7P	Black
			$C^7PO^{1/2}$	Yellow			

Upon variation of geometric parameters indicated in Table S1, some of the resulting conformations had too high energy (1.25 eV above equilibrium), i.e. were highly improbable. Such conformations are shown with "x" signs in Figure S5 and corresponding dashed lines. The obtained dependencies of A_P vs. $\cos^2\theta$ all show closely linear correlations and reasonably small deviation from the equilibrium curve, with exceptions for the above-mentioned highly improbable conformations.

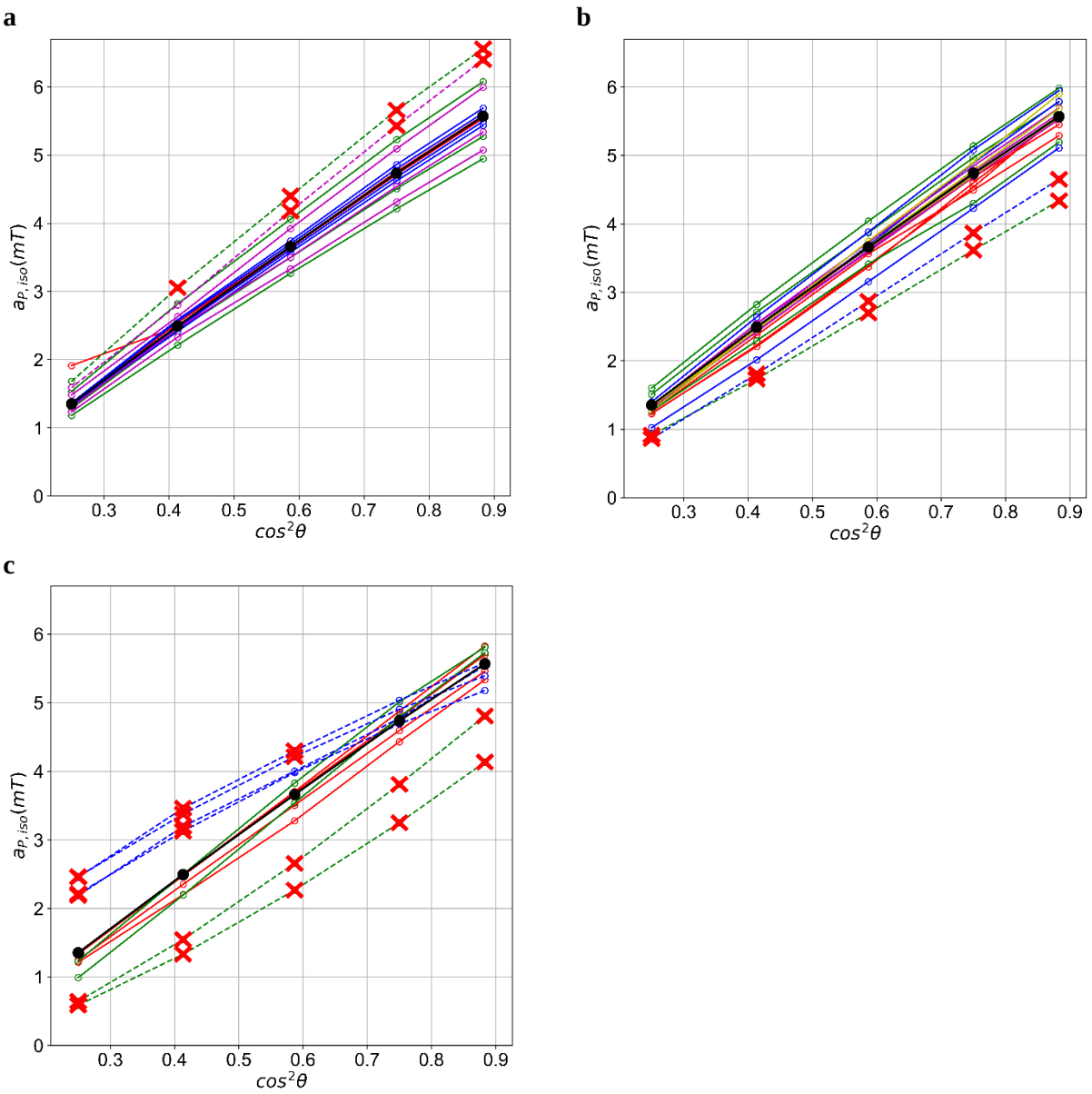

Figure S5. Dependence of A_P on $\cos^2\theta$ upon variation of the geometric parameters of the radical: (a) bond lengths, (b), angles (c) dihedrals. Points corresponding to low-probability radical conformations are marked with "x" signs and connected by dashed lines.

An important conclusion following the results of Fig.S5 is that in all cases the correlation of A_P with $\cos^2\theta$ is maintained, and (excluding the most improbable conformations) the absolute deviations of A_P upon variations of geometry are relatively small (on the order of 30%). At the same time, the theoretical (extrapolated) changes of A_P vs. $\cos^2\theta$ reach factor of 4 within $\cos^2\theta$ = [0.25 0.88], and experimental data confirms changes by a factor of ~2 within $\cos^2\theta$ = [0.3 0.7] (Fig. S4). Thus, we safely assume that all other geometrical changes have minor influence on the A_P value, whereas the dominant role of θ is undoubted.

In addition, we have examined the range of typical geometrical differences that S1 undergoes in solvents of different polarity. For this sake, the geometry of S1 was optimized in

methanol (E_N^T= 0.762) and toluene (E_N^T=0.099); then, angles and bond lengths (the same as given in Table S1) were compared. Dihedrals were not considered as they automatically change together with θ vs. polarity. In this calculation we again used B3LYP with RIJCOSX approximation, the def2/J auxiliary basis set; CPCM method was applied to set the polarities of methanol and toluene. Table S2 summarizes the obtained data.

Table S2. Selected angles and bond lengths for S1 optimized in methanol and in toluene. Relative differences from equilibrium state without solvent are given in each case.

Bonds	**Without solvent / A**	**In methanol / A**	**Difference / %**	**In toluene / A**	**Difference / %**
NO[4]	1.281	1.284	0.195	1.283	0.097
NC[7]	1.502	1.510	0.551	1.514	0.775
PO[3]	1.497	1.504	0.472	1.501	0.269
PC[7]	1.892	1.890	0.084	1.886	0.276
Angles	**Without solvent / °**	**In methanol / °**	**Difference / %**	**In toluene / °**	**Difference / %**
O[4]NC[8]	113.417	113.258	0.159	115.064	1.647
O[4]NC[7]	115.328	115.879	0.551	114.198	1.130
NC[7]P	107.009	108.406	1.397	112.929	5.920
C[7]PO[3]	114.965	117.328	2.363	116.860	1.895
C[7]PO[1/2]	100.667	100.112	0.555	98.696	1.971

As follows from Table S2, it was obtained that maximum changes in angles (other than θ) do not exceed 6%, and maximum changes in bond lengths do not exceed 1%. At the same time, such variations lead to the θ changes within 5%. Therefore, we believe that the realistic geometrical changes (other than θ angle) in S1 radical lead to completely negligible (within 5%) changes in θ angle. Our consideration (Fig. S5) of such huge deviations as 30 degrees for angles and 5% for bond lengths is a very strong exaggeration provided to show that even with such unrealistically huge geometry changes A_P value changes only moderately. Under more realistic assumptions (<6% changes in angles and <1% for the bond lengths) the changes of A_P lie within 5%. Thus, except for the θ angle, the changes of other angles and bond lengths in S1 vs. polarity have minor influence on the discussed phenomena.

III. Pulse EPR (ESEEM) studies

An additional way to verify whether indeed alcohol molecules in the cavity of ZIF-8 become oriented with OH groups toward center of the cavity (where radical resides, as is sketched in Figure 5 of the main text) is to perform pulse EPR (Electron Spin Echo Envelop Modulation, ESEEM) measurements with partly deuterated alcohols. This idea follows earlier work of Kevan et.al. [J. Phys. Chem. 1989, 93, 317-322] and relies on the measurement of the electron(radical) – deuteron(solvent) hyperfine interactions via characteristic deuterium ESEEM peak. Indeed, if we use partly deuterated methanol (as an example), CH_3OD, then we can hope to observe differences in deuterium ESEEM in two situations: (i) CH_3OD molecules are randomly oriented around the radical, as is presumably in the bulk solvent, or (ii) CH_3OD molecules are preferentially directed with OD-groups toward radical, as is supposed in ZIF-8 (Figure 5). One might expect that in the second case (ii) average OD-ON distances will be shorter and the deuterium peak will become broader.

In order to perform this experiment, we first synthesized partly deuterated methanol CH_3OD using the following procedure. Protonated methanol was mixed and stirred with D_2O to induce proton-deuteron exchange in OH group, then distilled and analyzed by NMR. NMR measurements were performed on Bruker AVANCE III HD spectrometer operating at 300 MHz (^{1}H Larmor frequency). To determine -CH_3:-OH protons ratio, 500 μL of the solvent (CH_3OH and CH_3OD) was transferred to an NMR tube. The ratio was determined based on the integrals of -CH_3 and –OH (Figure S6), eventually showing the huge excess of CH_3OD.

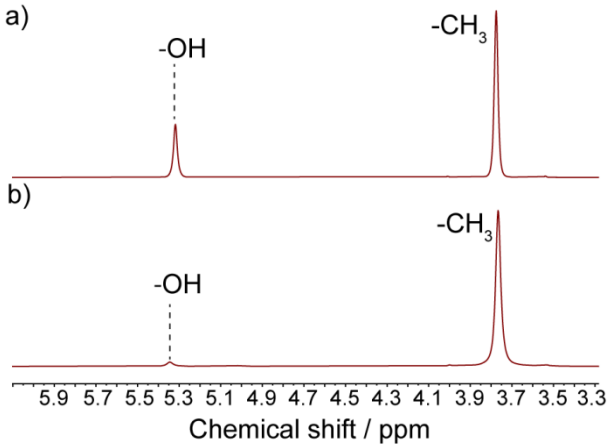

Figure S6. NMR spectra of CH_3OH (reference, a) and CH_3OD (synthesized, b).

Next, we performed three-pulse ESEEM measurements (80 K) in identical conditions for S1 radical dissolved in bulk CH_3OD and for S1@ZIF-8 impregnated with CH_3OD. The time delay between first two pulses was adjusted to the maximum of deuterium modulation at X-band (around

220 ns), all time delays and processing of ESEEM time-traces were kept exactly the same for two samples. Figure S7 shows the obtained frequency-domain data.

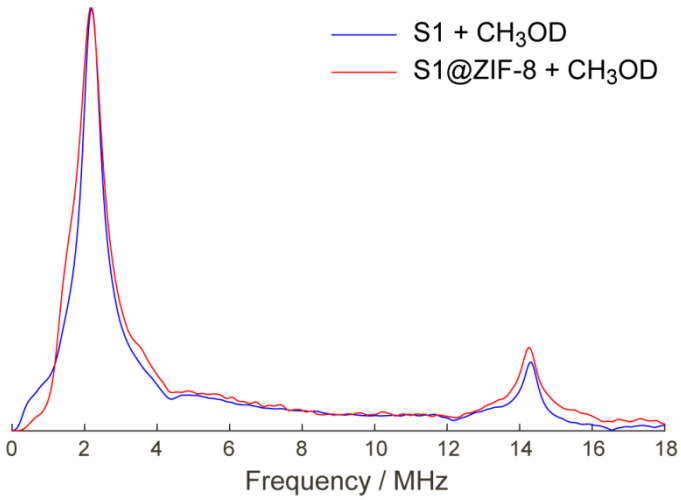

Figure S7. Frequency-domain 3pESEEM spectra of S1 radical dissolved in bulk CH_3OD (blue) and S1@ZIF-8 impregnated with CH_3OD (red).

The observed spectra are essentially the same. In fact, very small broadening can be seen for S1@ZIF-8 impregnated with CH_3OD, which is the anticipated trend. Certainly, such small difference cannot be considered as an ultimate proof-of-the-concept; however, at least it somewhat supports our interpretation on solvent nanoordering and certainly does not contradict it. In general, there can be many factors influencing the deuterium ESEEM peak in-MOF vs. in-bulk. For instance, even assuming that OD groups of CH_3OD all point toward the cavity center and the radical, the distances OD-ON can be slightly larger in MOF than in the bulk. Therefore, such comparison does not in principle guarantee solid conclusions on mutual location of radical and methanol in the MOF cavity.

IV. Details of multi-parameter simulations

In general form, equation (3) of the main text has to be written as:

$$\theta = \theta_0 + a_1 E_T^N + a_2 c + a_3 V_\mathrm{X} + a_4 V_\mathrm{M} \quad \text{(S2)}$$

Therefore, we have checked all main correlations following the scheme given by Table S3 below.

Table S3. Variation of parameters in eq.(S2) and the corresponding statistics.

eq.	***y*-intercept**[a,b]	a_1[b,c]	***t*-test**[c]	a_2[b,d]	***t*-test**[c]	a_3[b,e]	***t*-test**[c]	a_4[b,f]	***t*-test**[c]	R^2[g]	F[h]	N[i]
(i)	39.2 (14)	28.4 (25)	99.99	-[j]	-[k]	-[j]	-[k]	-[j]	-[k]	0.932	-[k]	11
(ii)	30.5 (16)	-[j]	-[k]	0.039 (3)	99.99	-[j]	-[k]	-[j]	-[k]	0.966	-[k]	9
(iii)	78.5 (36)	-[j]	-[k]	-[j]	-[k]	-0.45 (6)	99.99	-[j]	-[k]	0.856	-[k]	11
(iv)	76.6 (37)	-[j]	-[k]	-[j]	-[k]	-[j]	-[k]	-0.31(5)	99.99	0.835	-[k]	11
(v)	36.8 (17)	21.4 (40)	99.93	0.010 (5)	92.73	-[j]	-[k]	-[j]	-[k]	0.956	87	11
(vi)	53.7 (51)	19.1 (37)	99.92	-[j]	-[k]	-0.18 (6)	98.0	-[j]	-[k]	0.967	117	11
(vii)	**53.1 (37)**	**19.4 (28)**	**99.98**	-[j]	-[k]	-[j]	-[k]	**-0.13 (3)**	**99.52**	**0.976**	**165**	**11**
(viii)	50.6 (54)	19.5 (32)	99.93	0.003 (5)	47.00	-[j]	-[k]	-0.11 (4)	96.60	0.997	102	11

[a] Student *t*-test reliable at 99.99%. [b] Error given on the last digit. [c] Coefficient a_1 for E_T^N parameter. [d] Coefficient a_2 for c parameter. [e] Coefficient a_3 for V_X parameter. [F] Coefficient a_4 for V_M parameter. [g] Linear egression coefficient R^2. [h] *F*-test value at 99.99% reliability. [i] Number of data. [j] Not included. [k] Not estimated.

Linear and multi-parameter regressions have been performed using OriginPro 2023.

Note that E_T^N aliases polarity effect given by π* and hydrogen bonding effect, meaning that these parameters need not to be tested in multi-parameters correlations. Cohesive pressure c is used to test stiffness and structuredness of the solvation cage. This parameter is partly linked to the volume of the molecule which is either estimated by the molecular volume V_M or the intrinsic volume V_X. In general, c, V_X and V_M are not tested in common correlation. The best multi-parameter correlation is selected by combining the highest R^2 and F-test values, the highest reliable values of coefficient (Student *t*-test) with the lowest errors. Consequently, eqs. (i)-(v) are discarded due to the too low R^2, too low F-test and t-test values. Eq.(viii) is discarded because the reliability (*t*-test) on

the value of coefficient before *c* is lower than 50%. Eq.(viii) is preferred versus eq.(vi) only due to a slightly better statistics. Nonetheless, V_M and V_X report both on the effect of the size of the solvent.

Table S4 reports actual values used in our multi-parameter correlations.

Table S4. The values used in multi-parameter correlations.

θ^a	$E_T^{N\,b}$	c^b	$V_X{}^c$	$V_M{}^d$	solvent[e]	Number
38	0.009	205	81.3	114.52	*n*-pentane	**1**
43	0.009	205	81.3	114.52		
53	0.546	558	59	76.51	*i*-PrOH	**2**
55	0.617	600	59	74.8	*n*-PrOH	**3**
58	0.654	676	44.9	58.41	EtOH	**4**
61	0.762	858	30.8	40.43	MeOH	**5**
62	0.790	1050	50.8	56.01	EG	**6**
62	0.898	573	41.5	72.4	TFE	**7**
37	0.009	225	95.4	130.5	*n*-hexane	**8**
48	0.009	225	95.4	130.5		
54	0.386	581	58.1	77.4	DMF	**9**
57	0.481	669	42.4	53.64	$MeNO_2$	**10**
46	0.207	359	62.2	81.14	THF	**11**

[a] Given by eq.2 in manuscript.
[b] Given in C. Reichardt, T. Welton, Solvent and Solvent Effect in Organic Chemistry, 4th ed., Wiley-VCH, Weinheim, 2011.
[c] Given in Y. Marcus, *The Properties of Solvents*, Vol. 4, Wiley, Chichester, 1998.
[d] Given in G. E. Zaikov, R. G. Makitra, G. G. Midyana, L. I. Bazylyak, *Influence of the Solvent on Some Radical Reaction* Chemistry Research and Applications Series, Nova Science Publishers Inc., New York, **2010**
[e] *i*-PrOH: isopropanol; *n*-PrOH: propan-1-ol; EG: ethylene glycol; TFE: 2,2,2-trifluoroethanol; DMF: dimethylformamide, $MeNO_2$: nitromethane; THF: tetrahydrofurane.

Figures S8-S10 report the corresponding plots of the multi-parameter correlations.

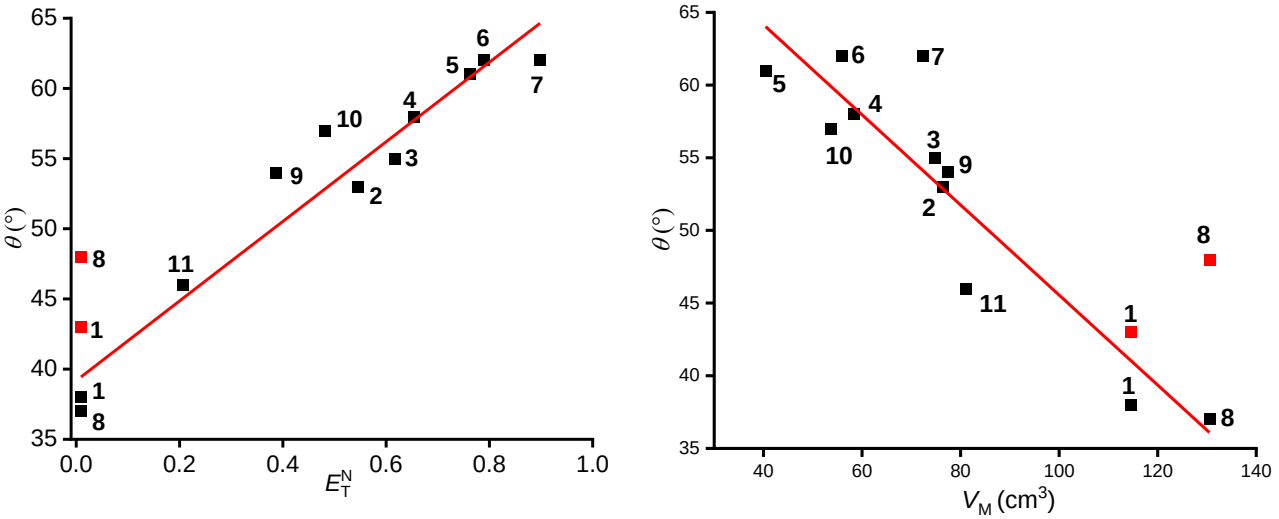

Figure S8. Plot E_T^N vs θ for solvent **1 – 11**. In red second isomer observed in **1** and **8**.

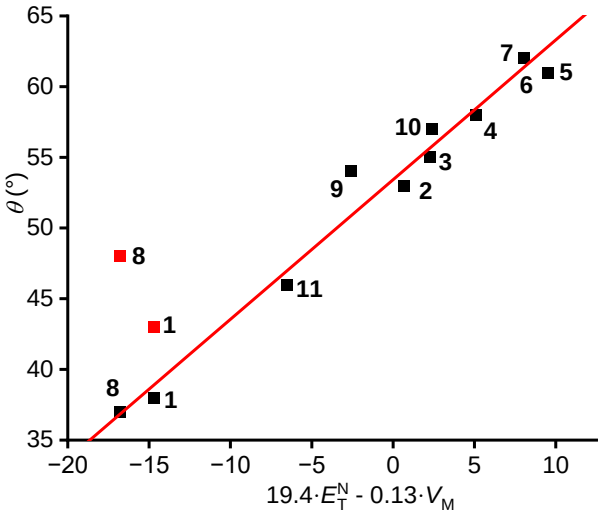

Figure S10. Plot $f(E_T^N, V_M)$ vs θ for solvent **1 – 11**. In red second isomer observed in **1** and **8**.

Figure S9. Plot V_M vs θ for solvent **1 – 11**. In red second isomer observed in **1** and **8**.

V. Additional EPR data and simulation parameters

Figure S11 shows additional CW EPR data for S1@ZIF-8 impregnated with non-hydrogen bonding solvents.

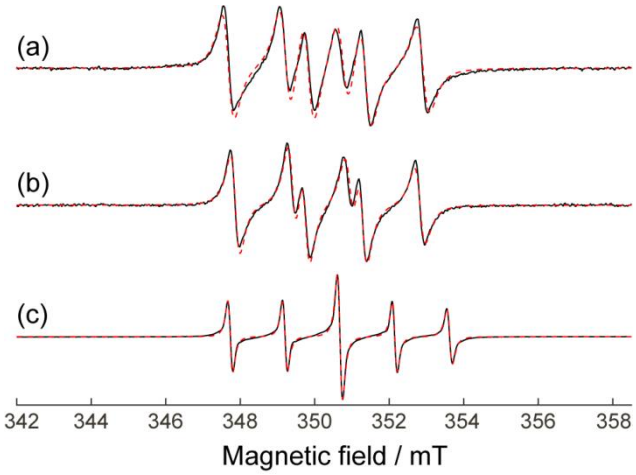

Figure S11. X-band room-temperature CW EPR spectra of S1@ZIF-8 impregnated by: N,N-dimethylformamide (a), nitromethane (b), tetrahydrofurane (c). Experimental spectra are shown in solid black lines, simulations in dotted red lines.

Table S5 reports all major parameters used in simulations of the CW EPR spectra shown in Figures 3, 7 and S11. Note that in Tables 1 and 2 we report isotropic ^{14}N HFI constants, to comply with theoretical approaches developed for the analysis of β-phosphorylated nitroxides earlier. The rotational correlation time (τ_c) and ^{14}N HFI anisotropy need to be taken into account only to better fit the intensities of the EPR lines, while the splittings at current small τ_c values are not yet influenced by HFI anisotropy. ^{14}N HFI tensor was typical for nitroxides (verified by low-temperature data on S1) and taken for each solvent to provide correspondence with the isotropic HFI value. It was not necessary to consider the ^{31}P HFI anisotropy, as it is usually small for β-atoms.

Table S5. Simulation parameters, including HFI anisotropy and rotational correlation times. g-tensor was taken g=[2.0098 2.0068 2.0027] in all cases.

solvent	**A_N / mT A_{XX} A_{YY} A_{ZZ}**	**A_P / mT**	**τ_c / ns**	**weight**
S1@ZIF + isopropanol	[0.65 0.65 3.242]	2.271	0.22	-
S1@ZIF + propanol	[0.65 0.65 3.260]	2.038	0.19	-
S1@ZIF + ethanol	[0.65 0.65 3.305]	1.840	0.28	-
S1@ZIF + methanol	[0.65 0.65 3.329]	1.543	0.16	-
S1@ZIF + ethylene glycole	[0.65 0.65 3.395]	1.470	0.19	-
S1@ZIF +TFE	[0.65 0.65 3.380]	1.430	0.21	-
S1@ZIF open to air	[0.65 0.65 2.960]	4.033	0.06	-
S1@ZIF + dimethylformamide	[0.65 0.65 3.320]	2.160	0.17	-

S1@ZIF + $MeNO_2$	[0.65 0.65 3.320]	1.890	0.19	-
S1@ZIF + tetrahydrofurane	[0.65 0.65 3.125]	2.955	0.10	-
S1@ZIF + hexane	[0.65 0.65 2.993]	3.798	0.18	0.45
	[0.65 0.65 3.095]	2.723	0.56	0.55
S1@ZIF + pentane	[0.65 0.65 2.993]	3.798	0.14	0.45
	[0.65 0.65 3.095]	3.218	0.14	0.55